A Multibody Dynamics-Enabled Mobility Analysis Tool for Military Applications

Daniel Melanz, Hammad Mazhar, and Dan Negrut

1 Abstract

This paper describes a modeling, simulation, and visualization framework aimed at enabling physics-based analysis of ground vehicle mobility. This framework, called Chrono, has been built to leverage parallel computing both on distributed and shared memory architectures. Chrono is both modular and extensible. Modularity stems from the design decision to build vertical applications whose goal is to reduce the end-to-end time from vision-to-model-to-solution-to-visualization for a targeted application field. The extensibility is a consequence of the design of the foundation modules, which can be enhanced with new features that benefit all the vertical applications. Two factors motivated the development of Chrono. First, there is a manifest need of modeling approaches and simulation tools to support mobility analysis on deformable terrain. Second, the hardware available today has improved to a point where the amount of sheer computer power, the memory size, and the available software stack (productivity tools and programming languages) support computing on a scale that allows integrating highly accurate vehicle dynamics and physics-based terramechanics models. Although commercial software is available nowadays for simulating vehicle and tire models that operate on paved roads; deformable terrain models that complement the fidelity of present day vehicle and tire models have been lacking due to the complexity of soil behavior. This paper demonstrates Chrono's ability to handle these difficult mobility situations through several simulations, including: (i) urban operations, (ii) muddy terrain operations, (iii) gravel slope operations, and (iv) river fording.

2 Introduction

Despite the integral role that off-road vehicles play in combat and military operations, researchers do not currently have the ability to accurately (i) estimate vehicle operational parameters such as forces, torques, and sinkage that a wheel or track on a vehicle experiences, (ii) investigate the interaction that occurs between a wheel/track and soft soil, and (iii) simulate a ground vehicle's ability to navigate complex off-road terrain. Deformable terrain models that complement the fidelity of present day vehicle and tire models have been lacking due to the complexity of soil behavior. In the context of soil dynamics, terramechanics models fall into three categories of increasing complexity as they rely on methods that are: (i) purely empirical, (ii) semi-analytical, or (iii) physics-based approaches. Purely empirical terrain models, such as Bekker, Wong, and NRMM, typically used for "go/no-go" vehicle mobility assessment, have several drawbacks: the parameters can be sensitive to experimental testing procedures, they do not scale well to vehicles with small contact patches, they expose only a small number of model parameters, and they cannot capture 3D effects manifested at the interface between wheel/track and terrain [1]–[3]. Semi-analytical terramechanics models, such as Ayer's [4], have been applied with limited success for general purpose vehicle mobility simulations in off-road conditions since: (a) tire geometry is most often assumed to be simple and described in two-dimensions, which does not capture tread/lug geometry effects on tractive performance, and (b) soil flow effects (e.g., bulldozing, slip sinkage, rutting) are also generally ignored or dealt with in an ad-hoc manner. The third approach, which is the focus of this paper, draws on physics-based methods, such as mesh-less, finite element, and discrete element, which are currently prohibitively expensive due to a large amount of data computation and movement that they require.

At one end of the Computer Aided Engineering (CAE) spectrum, there are commercial Discrete Element Method (DEM) codes that concentrate on dry-friction governed granular dynamics [5], [6]. These codes can be used to investigate the dynamics of one to two million body systems. However, they cannot handle modeling and numerical solution challenges posed by highly nonlinear multibody systems such as robots, tractors, tracked vehicles, etc., whose dynamics is captured by systems of index-3 Differential Algebraic Equations (DAEs) [7]–[9]. At the other end of the spectrum, these DAE problems are routinely solved by computational multi-body dynamics (CMBD) commercial packages such as ADAMS, SimPack, or RecurDyn [10]–[12]. Yet CMBD packages handle large frictional contact problems posed by discrete media dynamics poorly. For instance, a test was conducted first in 2007 [13] and repeated in 2013 [14] to gauge the scalability of a widely used commercial CMBD package. The conclusion was that a three second simulation of a dynamics problem with one million bodies would require tens of years of compute time in both the 2007 and 2013 versions of commercial solution. However, virtual prototyping in engineering requires analysis of complex vehicles operating with/on discrete systems with billions of bodies. After all, in one cubic meter of sand there are more than one billion elements. Driving over or moving around one cubic meter of sand cannot be simulated today due to the inability of the existing DEM and CMBD solutions to handle the size and bridge the scales that manifest in the physics of interest. However, recent advances in computing technology provide a fresh opportunity to reconsider this approach.

To carry out one million floating point operations in one second (1 MFLOP/s) would have required in 1961 the requisition of 17 million IBM-1620 computers. At $64K apiece, when adjusted for inflation this would come out at half the 2013 US national debt. The price came down to around $1,000 in 2000. Today, only 20 cents of the value of a desktop would be used to yield 1 MFLOP/s. The packing of an increasing number of transistors per unit area, which is expected to continue according to Moore's law at least until 2021, demonstrates manifestly that the barrier to solving large-scale CMBD problems of relevance in Science and Engineering is lack of modeling techniques and solution methods that leverage advanced computing hardware. A back of the envelope calculation suggests that a problem with 1 billion bodies roughly requires memory on the order of 1 TB: 1 billion bodies times 8 bytes (double precision) times 100 variables per body (positions, velocities, accelerations, moments of inertia, bilateral constraints, etc.). In two years, 1 TB of memory and 5,000,000 MFLOP/s; i.e., 5,000 billion operations per second, is what an engineer will have access to on a high-end workstation tucked under the desk.

In the light of this discussion, this paper describes a modeling, simulation, and visualization framework, called Chrono, aimed at enabling high performance, physics-based, analysis of ground vehicle mobility. The paper is organized into two parts: Section 3 describes the Chrono software and the setup of several mobility scenarios, specifically urban operations, muddy terrain operations, gravel slope operations, and river fording; and Section 4 details some example engineering studies that can be taken from the simulated mobility situations.

3 Methodology

3.1 Chrono: An End-to-End Mobility Toolkit

3.1.1 Implementation

Project Chrono is an open-source general purpose simulator for large-scale, three-dimensional, multibody dynamics problems [15]. The core of Project Chrono is the Chrono::Engine C++ middleware, a powerful object-oriented set of libraries whose application program interface (API) can be freely used to develop simulation software . Specifically, the code is designed to support the simulation of very large systems such as those encountered in granular dynamics, where the number of interacting elements can be in the millions. Figure 1 illustrates the architecture of Chrono. Based on third–party, open source, and in-house developed code, it represents an end-to-end solution to large-scale dynamics problems. It relies on CUDA for GPU computing, OpenMP for many-core shared memory computing, and MPI for multi-socket distributed memory computing to implement fine, medium, and coarse-grain parallelism across the modeling, simulation, and visualization stages of an analysis. Its foundation consists of five basic components that provide support for: (1) modeling; (2) numerical solution; (3) proximity computation and contact detection; (4) domain decomposition and inter-domain communication; and (5) pre/post-processing.

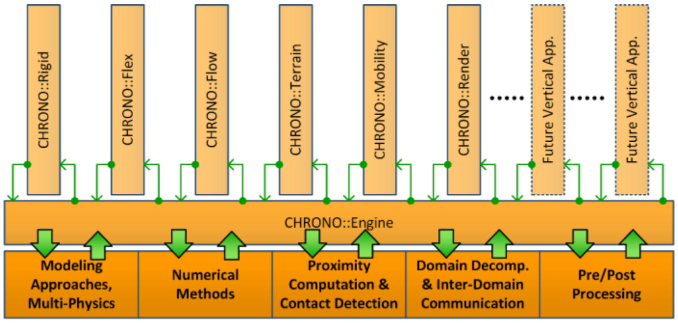

Figure 1: The Chrono parallel computing infrastructure.

The modeling component formulates the set of equations that govern the dynamics of the system of interest. The numerical solution component provides the parallel algorithmic support required to solve this set of equations. Depending on the underlying physics, various parallel solvers are employed for: optimization problems arising in a Differential Variational Inequality (DVI) approach for handling frictional contact; solving nonlinear problems arising in the context of implicit numerical integration; SPH-based methods for fluid-solid interaction problems, etc. For discrete problems, the proximity computation and contact detection component handles contact detection tasks; for continuum problems handled in a mesh-less framework it produces the list of neighboring nodes that overlap the compact support associated with each node of the discretization. The domain decomposition and inter-domain communication component handles the splitting of large problems into subdomains and managing in a transparent fashion the inter-process communication. Finally, the pre/post-processing component supports the process of setting up a model using the Chrono API and gaining insights into the rich dynamics of a ground mobility problem through visualization of the simulation.

3.1.2 Theory

Chrono requires a small number of model parameters, allows for integration at large step-sizes, and robustly handles the discontinuities in velocities but calls for more involved mathematical instruments both in the equation formulation and equation solution stages. The concept of equations of motion is extended to include differential inclusions [16]. The simplest example is a body that interacts with the ground through friction and contact, for which the equations of motion assume the form $\mathbf{M}\ddot{\mathbf{q}} + \mathbf{g}_{\mathbf{q}}^{\mathrm{T}}\boldsymbol{\lambda} - \mathbf{f} \in \mathbf{F}(\mathbf{q},t)$, where $\mathbf{M}$ is the inertia matrix, $\ddot{\mathbf{q}}$ is the rigid body acceleration, $\mathbf{g}_{\mathbf{q}}^{\mathrm{T}}\boldsymbol{\lambda}$ is the reaction force due to any bilateral kinematic constraints acting on the body, $\mathbf{f}$ is the external force, and $\mathbf{F}(\mathbf{q},t)$ is a set-valued function. For frictional contact problems, the inclusion above states that the frictional contact force lies somewhere inside the friction cone, with a value yet to be determined and controlled by the stick/slip state of the interaction between body and ground. In CMBD the differential inclusion can be posed as a DVI problem [17]. In its most general form, it assumes the form in Figure 2 [18]–[20], which has been proved to resolve Painlevé's paradox [17].

Referring to the boxes at the left in Figure 2, the *Kinematic Differential Equations* provide the connection between the generalized velocities and the time derivative of the generalized positions. The right hand side of the *Force Balance Equations* represent the generalized forces acting on the rigid bodies: external forces (e.g., gravity or a torque applied to a driving wheel); the reaction forces associated with the bilateral constraints (kinematic joints) present in the system; and the contribution of the frictional contact forces (two tangential components and a normal component). The bilateral constraints are expressed next as a set of *Holonomic Kinematic Constraints*; that is, a collection of nonlinear algebraic equations that involve the generalized positions and possibly time. Unilateral constraints define a set of *Contact Complementarity Conditions*, which indicate that either the gap between two geometries that define contact i is zero and consequently the associated Lagrange multiplier is greater than zero, or vice versa. Finally, the last set of equations poses an optimization problem whose first order Karush-Kuhn-Tucker (KKT) optimality conditions [21] are equivalent to the *Coulomb Friction Model*.

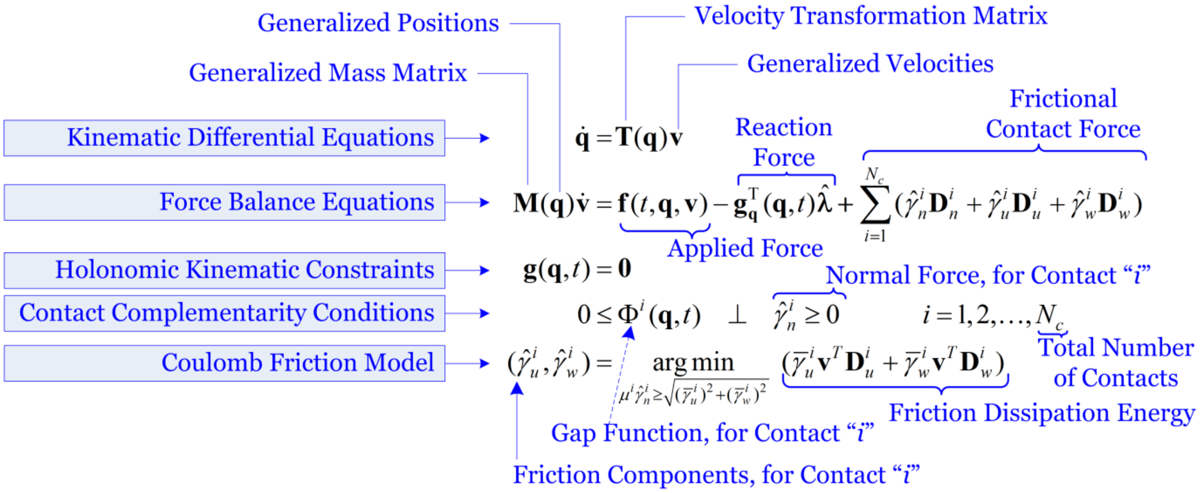

Generalized Positions
Velocity Transformation Matrix
Generalized Mass Matrix
Generalized Velocities
Frictional Contact Force
Reaction Force
Kinematic Differential Equations
Force Balance Equations
Holonomic Kinematic Constraints
Contact Complementarity Conditions
Coulomb Friction Model
$\dot{\mathbf{q}} = \mathbf{T}(\mathbf{q})\mathbf{v}$
$\mathbf{M}(\mathbf{q})\dot{\mathbf{v}} = \mathbf{f}(t,\mathbf{q},\mathbf{v}) - \mathbf{g}_{\mathbf{q}}^{T}(\mathbf{q},t)\hat{\boldsymbol{\lambda}} + \sum_{i=1}^{N_c}(\hat{\gamma}_n^i\mathbf{D}_n^i + \hat{\gamma}_u^i\mathbf{D}_u^i + \hat{\gamma}_w^i\mathbf{D}_w^i)$
Applied Force
$\mathbf{g}(\mathbf{q},t) = \mathbf{0}$
Normal Force, for Contact "i"
$0 \le \Phi^i(\mathbf{q},t) \quad \perp \quad \hat{\gamma}_n^i \ge 0 \qquad i = 1,2,\ldots,N_c$
Total Number of Contacts
$(\hat{\gamma}_u^i, \hat{\gamma}_w^i) = \underset{\mu^i\hat{\gamma}_n^i \ge \sqrt{(\bar{\gamma}_u^i)^2+(\bar{\gamma}_w^i)^2}}{\arg\min} (\bar{\gamma}_u^i\mathbf{v}^T\mathbf{D}_u^i + \bar{\gamma}_w^i\mathbf{v}^T\mathbf{D}_w^i)$
Friction Dissipation Energy
Gap Function, for Contact "i"
Friction Components, for Contact "i"

Figure 2: DVI formulation of the CMBD problem with friction and contact [22], [23]**.**

The DVIs in Figure 2 are discretized to yield the mathematical program with complementarity and equality constraints shown in Figure 3. The discretization is based on a symplectic half-implicit Euler method [24], which advances the state of the system from time $t^{(l)}$ to $t^{(l+1)}$ using a step size *h*. This discretization was proposed in [18] and yielded a first order scheme. Subscripts represent partial derivatives while a superscript in parenthesis represents the time step at which the variable is evaluated. The instantaneous Lagrange multipliers were scaled to become constraint reaction impulses: $\lambda \equiv h\hat{\lambda}$; for the normal and two tangential friction forces, $\gamma_\alpha \equiv h\hat{\gamma}_\alpha$ for $\alpha = n,u,w$.

To the best of our knowledge, no numerical method has been demonstrated to reliably solve a sizeable problem of this type; i.e., a problem that combines nonlinear algebraic equations with complementarity conditions and with a large number of coupled optimization problems that provide for the friction force. The coupling occurs through the normal forces which enter both the *Coulomb Friction Model* and the *Contact Complementarity Conditions*. This large problem must be solved at every integration time step.

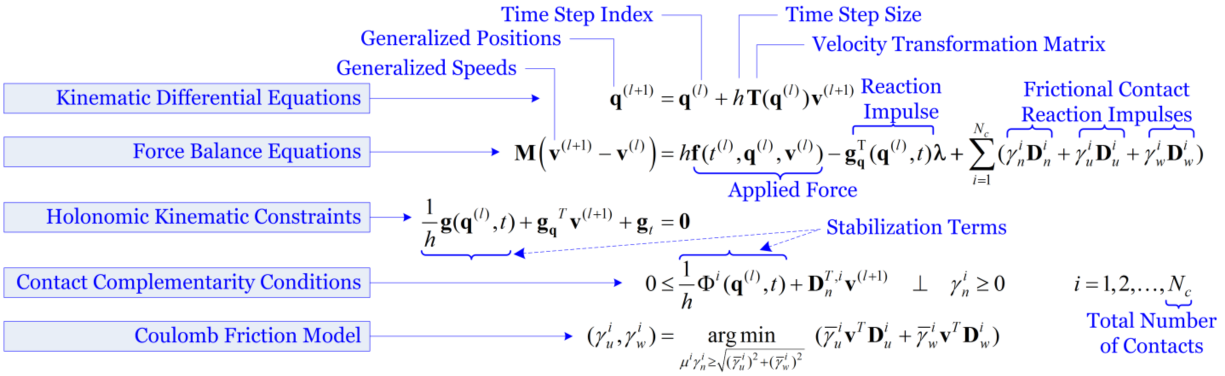

Figure 3: Discretization of the DVI problem into a mathematical program with complementarity and equality constraints [25], [26]**.**

For instance, consider the dynamics of a rover moving over a granular system with 1 million discrete bodies. This calls for approximately: six million equations coming out of the *Kinematic Differential Equations*, another six million for the *Force Balance Equations*, several hundred *Holonomic Kinematic Constraints* associated with the rover model, about three to four million complementarity conditions for the normal force, and the same number of conditions for the *Coulomb Friction Model*.

Two relaxations of this numerical problem have gained wide acceptance. The first draws on a linearization that turns the friction cone into a pyramid [18], [26], [27]. On the upside, once the kinematic constraint equations are also linearized, the problem becomes a Linear Complementarity Problem (DVI-LCP). On the downside, the dimension of the problem balloons: while typically three unknowns are associated with a frictional contact (one normal force and two components of the friction force in the tangent plane), the number of unknowns is now proportional to the number of facets in the pyramid. If this number is low, artificial anisotropy is induced into the system dynamics. The second approach to relaxing the problem in Figure 3 sets out by asking the following question: what modification should one make to this problem to turn it into a Cone Complementarity Problem (CCP)? Although algorithms for solving CCPs are not as straightforward or ubiquitous as the ones for LCPs, such problems can be reformulated and solved as quadratic optimization problems with conic constraints [28]. Replacing the *Contact Complementarity Conditions* with

$$0 \le \frac{1}{h}\Phi^i(\mathbf{q}^{(l)},t) + \mathbf{D}_n^{T,i}\mathbf{v}^{(l+1)} - \mu_i\sqrt{(\mathbf{D}_u^{T,i}\mathbf{v})^2 + (\mathbf{D}_w^{T,i}\mathbf{v})^2} \quad \perp \quad \gamma_n^i \ge 0 \qquad i = 1,2,\ldots,N_c$$

yields the following CCP: at each time step, given a matrix $\mathbf{N} \equiv \mathbf{D}^T\mathbf{M}^{-1}\mathbf{D}$ and vector $\mathbf{r}$, find a vector $\mathbf{z}$ of Lagrange multipliers so that $\mathbf{z} \in \Gamma \perp (\mathbf{N}\mathbf{z} + \mathbf{r}) \in \Gamma^*$. Here, Γ is the friction hyper-cone of dimension 3N$_c$; Γ^* is the dual hyper-cone of Γ; $\mathbf{D}$ is obtained by splicing together the column vectors $\mathbf{D}_n^i$, $\mathbf{D}_u^i$, and $\mathbf{D}_w^i$ for $i = 1,2,\ldots,N_c$, and $\mathbf{r}$ is a vector that accounts for the external forces and information from the previous time step [29]. The resulting DVI-CCP method approximates well at large time steps h the solution of the original numerical problem as long as the friction and/or relative velocities at the point of contact are small. Moreover, it was shown in [28] that when $h \to 0$, the relaxed problem converges to the same measure differential inclusion as the original numerical problem. Iterative algorithms, based on fixed point iteration and projected Gauss-Seidel with successive over-relaxation, have been proposed for the solution of the relaxed problem [19], [30], [31].

3.1.3 Validation Efforts

The DVI approach was validated against flow rate and angle of repose experimental data in [32]. An aluminum rig was designed and fabricated to measure the gravity-induced mass flow rate through a slit (gap) of a specified amount of granular material (Figure 4). The flow of the 500 micron diameter glass spheres was simulated for each slit size used in the lab experiments (1.5, 1.6,…, 3 mm). Figure 4 shows the simulation results plotted next to experimental measurements (weight as a function of time). Good statistical correlation; i.e., less than 3% error, was observed between simulation and experimental results [33].

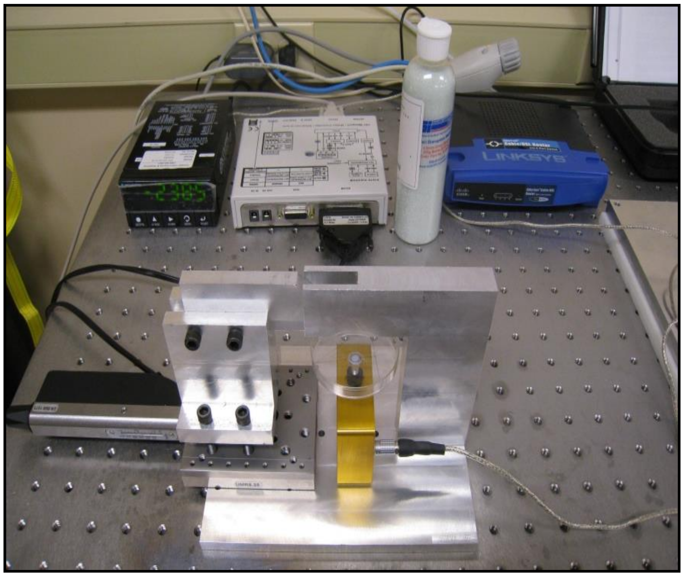

Figure 4: Experimental setup (left), simulation snapshot, and plot with comparison of numerical and experimental results. Approximately 39,000 monodisperse glass spheres of 500 µm diameter were used in the experiment [33].

A second DVI validation test was recently run for an impact problem in a series of simulations reported in [34]. A relation of the form $d = 0.14/\mu\sqrt{\rho_b/\rho_g}\,D_b^{2/3}H^{1/3}$ has been empirically established [35], where d is the depth of penetration, h is the height from which a ball of density ρ_b and diameter D_b is dropped, $H = d + h$ is the total drop distance, and ρ_g is the density of the granular material. Finally, μ was the friction coefficient in the granular material obtained from an angle of repose experiment as $\mu = \tan(\theta_r)$, where θ_r is the repose angle. As reported in detail in [34] for this impact problem, the simulation error was on the order of 13.7%. In this test, the emergent behavior, i.e. the empirical equation above, is the result of the coordinated motion of 0.5 million bodies.

3.2 Mobility Models

Military maneuvers, involving tactical formations and movements of wheeled and tracked vehicles across a landscape, provide the edge in combat for military units. However, scientists and engineers, who most often design the vehicle-weapons systems capabilities used in combat operations, are generally not included in the tactical planning process and must design vehicles based on expected mobility challenges. It is difficult and expensive to evaluate a vehicle’s performance during a majority of military maneuvers using experiments. The Chrono framework provides an end-to-end mobility toolkit to simulate a variety of mobility models to investigate the performance of a vehicle during common military maneuvers, such as urban, muddy terrain, gravel slopes, and river fording operations.

3.2.1 Urban Operations

Historical and much of modern guidance are consistent: avoid urban warfare if possible. Numbers of casualties are very high; consumption of ammunition and other supplies far exceeds that in most other environments; leader control of combat operations is limited [36]. Cities include some of the world's most difficult terrain in which to fight. The combinations of tactics, assaulting forces, enemy dispositions, and arrangement of non-combatants that could be experienced in an urban environment are immense [37]. Unfortunately, Armed forces are ever more likely to fight in cities as the world becomes increasingly urbanized [36]. Future battles will more likely ensue on the city streets than on the conventional terrains of the past. Mogadishu in Somalia, Grozny in Chechnya, and Fallujah in Iraq were urban battles that might foreshadow future modern warfare [37]. Environmental clutter, in particular, poses a large hurdle for situation assessment in contemporary urban combat environments. The clutter factor arises from the fact that the environment can be populated with a large number and arbitrary mixture of adversarial and neutral entities [38]. Increased emphasis on urban environment computer simulations will result in improved preparation for maneuvering in city streets or within buildings [36]. Due to Chrono's ability to handle large amounts of collision and contact, it is possible to simulate deformable urban environments with dynamic clutter.

A brick wall, shown in Figure 5, was modeled in Chrono to represent a common obstacle that military vehicles face in an urban environment. The model is composed of a rigid terrain with a wall composed of 150 bricks. Bricks are modeled as discrete bodies with a friction coefficient of 0.4 along with a varying cohesion between bricks to model the concrete forces. The bricks are created using a box collision geometry with dimensions 0.8 m by 0.4 m by 0.792 m for the length, height, and width, respectively. The tracked vehicle in the simulation has a total mass of 56,000 kg and is composed of 153 bodies, 138 of which are used to model the tracks. The tracks' collision geometry was created by a union of box primitives and the tank body was imported from a Wavefront .obj geometry file. An iterative CCP method with successive over-relaxations was used, with a simulation step-size of 0.005 seconds, to solve at each time step the system of equations in Figure 3.

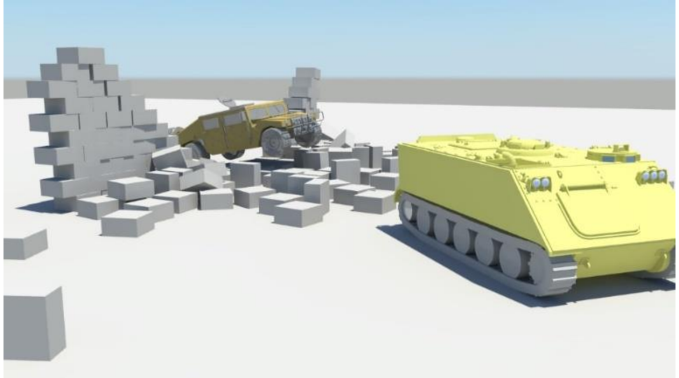

Figure 5: Urban operations.

3.2.2 Muddy Terrain Operations

Understanding muddy terrain operations is of great importance to military applications. It was found that depending on the amount of water present in the soil, the trafficability of wet soil, i.e. mud, can be better than dry soil. At a certain saturation state, soil becomes mud resulting in low shear forces and a higher chance of soil sticking to the wheel [39]. Highly saturated soils offer little resistance to wheel sinkage and can only support light vehicles. There are several problems that can occur while traversing mud, such as the cage wheel-blocking problem, where the wheel becomes completely laden with soil [40]. On the other hand, the weakened soil caused by high saturation is the main factor which causes the wheel to slip, sink and remain standstill [39]. Chrono can simulate mud using the discrete element method with particle to particle cohesion.

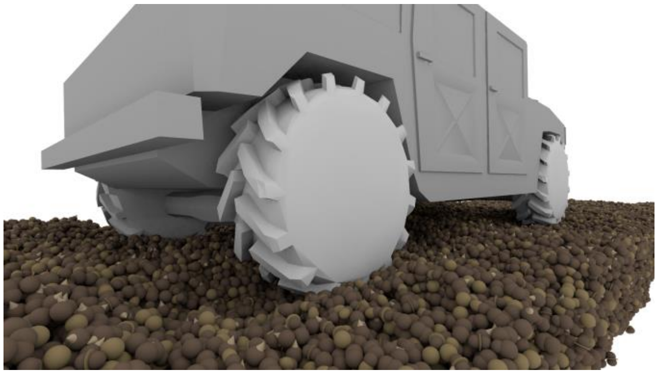

Figure 6: Muddy terrain operations.

The muddy terrain simulation consisted of a 3000 kg HMMWV and four rigid 60kg wheels with treads. Each wheel was rigidly attached to a fixed axle that was driven at a constant angular velocity of 1 rad/s. A bed of 200,000 objects of varying shape were created with a density of 1250 kg/m^3. Seven different compound shapes were used for the collision geometry, consisting of spheres, ellipsoids and cones. The rigid bodies interacted with a sliding friction value of .5 and a cohesion value of 25. The simulation was run on an Intel 4770K 4th generation Core i7 processor with 8 threads running in parallel. The time step was 1e-3 seconds and a total of 18 hours were needed to get 15 seconds of simulation. An iterative CCP solver based on the accelerated projected gradient descent method [34] was used with a maximum of 45 iterations at each time step. For this problem, the model leads to roughly three million equations in Figure 3.

Using this model, the sinkage of each wheel along with the reaction forces at each wheel spindle can be measured. Further improvements will incorporate a suspension into the vehicle so that the forces between the wheel and the chassis can be computed.

Additionally, a torque, rather than a constant angular velocity will be applied to the wheels so that the speed of the vehicle through the mud can be determined.

3.2.3 Gravel Slope Operations

Maneuvering on non-flat terrain is an important capability of military vehicles operating on off-road terrain [41]. Terrain with slopes exceeding 15° are considered steep slopes with vehicles typically being able to handle slopes up to 20° under favorable conditions. First studies of vehicle motion on slopes were published in the late 1960s [42]. Stability loss on rough slopes is more likely than on smooth slopes because the wheels follow the bumps and hollows of the rough ground and cause steep local slopes [43]. Some widely acknowledged cause of critical situations are: (i) overturning due to dynamic effects, lack of inherent stability or external load, (ii) sliding as the effect of excessive stress in the tire-ground contact area followed by a build-up of speed and eventual consequent overturn, and (iii) functional shortcomings of a vehicle (e.g. unsuitable engine, inadequate brakes, drivetrain, etc.) [42]. Chrono provides a means by which engineers can study a specific vehicle's performance on gravel slopes.

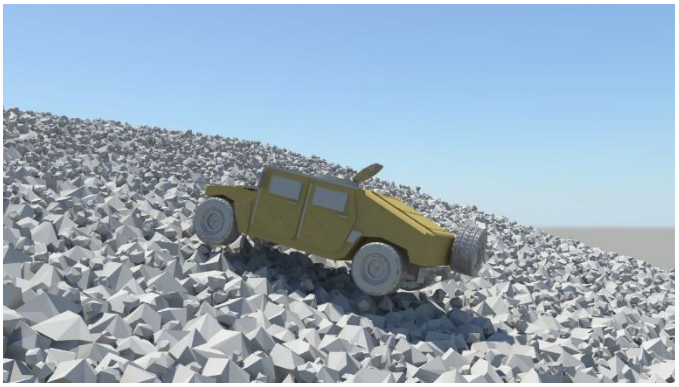

Figure 7: Gravel hill operations.

A rocky slope, shown in Figure 7, was modeled in Chrono to represent a common obstacle that military vehicles face in gravel hill operations. The terrain's slope varies from 14° to 20° and is composed of over 8,000 unique rocks with a randomly generated polyhedral collision geometry. Each rock was created by importing a Wavefront .obj model of a dodecahedron whose vertices was randomly perturbed to create a jagged, rock-like shape. Since perturbing these vertices often resulted in a non-convex collision geometry, convex decomposition was used to divide the rocks into convex sub-geometries. The final collision geometry for each rock was created from the union of its sub-geometries. The radius of the rocks varies from 0.2 m for the bedrock to 0.07 m for the tumbling rocks each having a coefficient of friction 0.4 and a density of 2.0 g/cm^3. The vehicle in the simulation has a total mass of 1500 kg and is composed of 13 bodies, including four rigid wheels. An iterative CCP solver with successive over-relaxations was used, with a simulation time step of 0.01 seconds. For this problem, the number of equations in Figure 3 is close to 0.2 million.

3.2.4 River Fording Operations

The requirement that military, combat, and tactical use vehicles have an inherent river-crossing ability has existed for some years [44]. River fording operations have to do with the ability of vehicles to function in and near waterways. River fording includes the regions on both river banks, the water in the river and the land under it [45]. If a vehicle does not have the capability to ford a river and there is no ford or bridge available it is necessary to build an improvised bridge, attach a fording kit to the vehicle, or by-pass the river completely [46]. Although most vehicles can handle rivers, it is desired to design faster and more efficient vehicles. Speed is elusive because of the severe drag and wave making properties implicit in box-shaped bodies. More and more power does not assure more speed, except in worthlessly small increments, but rather serves to make bigger and bigger waves [45]. Additionally, vehicles operating in water have the potential to become unstable. Without control the vehicle might float downstream in a whirling path and miss the target exit completely, or arrive at the exit still striving for directional precision [45]. Chrono has the ability to approximate fluid using low friction contact between particles, providing valuable insights into a vehicle's ability to cross a river.

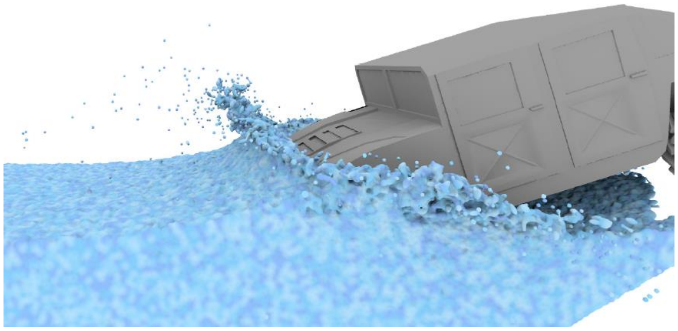

Figure 8: River fording operations.

The river fording simulation consisted of 200,000 frictionless spheres with a density of 1000kg/m^3 in a deep channel. The HMMVW is kinematically driven through the channel with the rigid wheels rotating at a constant speed of 1 rad/s. The chassis and wheel geometry are made up of triangle meshes. The time step for this simulation was .001s and it was simulated on an Intel 4770K 4th generation Core i7 processor with 8 threads running in parallel. Simulation time was 6 hours for 5 seconds of simulation. An iterative CCP solver based on the accelerated projected gradient descent method [34] was used with a maximum of 30 iterations performed per time step. For this problem, the number of equations in Figure 3 is roughly 3 million.

4 Results

This section details sample engineering analyses that can be performed to obtain output relevant in the context of military applications and ground mobility studies. For the urban investigation, the brick wall model described in Section 3.2.1 was used to perform a study on the tracked vehicle's ability to destroy the wall as the cohesive forces between the bricks were increased. For the muddy terrain investigation, the terrain described in Section 3.2.2, the cohesion of the mud was varied to understand how the vehicle speed changes as the soil becomes less cohesive. For the gravel slopes investigation, the slope of the hill described in Section 3.2.3 was varied to determine the wheeled vehicle's ability to climb the terrain. Lastly, for the river fording investigation, the river described in Section 3.2.4, the vehicle-water interaction was studied for different river heights.

4.1 Urban Investigation

A series of simulations was performed to investigate the tracked vehicle's ability to surmount an urban obstacle, specifically the brick wall shown in Figure 5. The tracked vehicle was aimed directly at the wall and propelled with a constant torque. The cohesive forces between the bricks in the wall were varied to determine what strength of the wall would prevent the tracked vehicle from smashing through the wall.

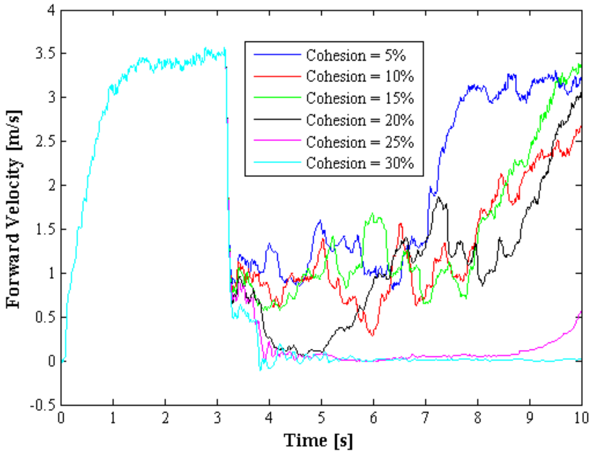

Figure 9: Forward velocity of the tank over time as a function of the brick cohesion. Collision between the tank and the wall occurs at approximately three seconds.

The forward velocity of the vehicle plotted over time is shown in Figure 9. Six simulations were performed with the cohesion of the brick wall ranging from 5 to 30%. The tracked vehicle starts at zero velocity and ramps up to a steady state velocity of approximately 3.5 m/s. The tracked vehicle collides with the brick wall at approximately three seconds, causing the vehicle to lose velocity. For low levels of cohesion, the tracked vehicle is able to easily surmount the obstacle. As the cohesion increases, however, it is more challenging for the vehicle to destroy the wall. For example, the vehicle is completely immobilized when the cohesion of the brick wall is set to 30%. The simulation was performed on a single core of an Intel Nehalem Xeon E5520 2.26 GHz processor. Being a relatively small model, the simulation took approximately 2 minutes to compute 10 seconds of vehicle dynamics.

4.2 Muddy Terrain Investigation

A set of simulations was performed to understand the vehicles' ability to traverse muddy terrain at decreasing values of inter-particle cohesion. The wheels of the vehicle were rotated at 1 rad/s and the sinkage and forward velocity of the chassis were measured. Figure 10 shows how the height of the chassis varies as the cohesion value for the terrain changes. As expected, for lower cohesion the height of the chassis is lower as the entire vehicle sinks into the ground. Note that the terrain is uneven causing the overall change in height of the chassis. Figure 11 shows the forward velocity of the vehicle as it drives on the terrain for two different cohesion values. Note how for the smaller cohesion value the speed of the vehicle varies more in comparison to the higher cohesion value. This is due to the vehicle having difficulty gripping the terrain causing it to slow down when it loses traction and speed up when it gains traction. For the larger cohesion value the vehicle always maintains better grip causing smaller fluctuations in velocity.

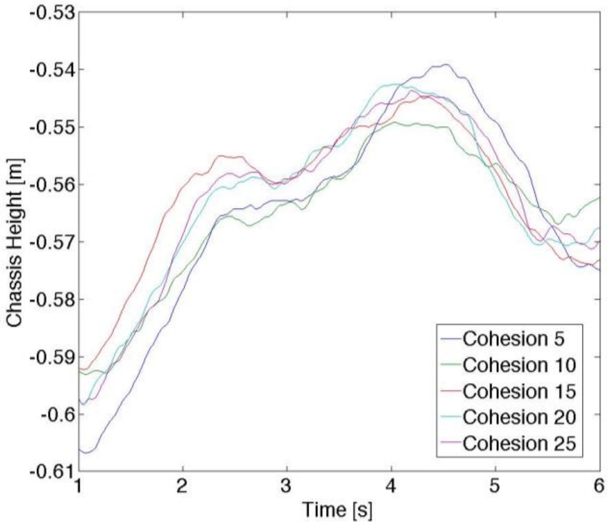

Figure 10: Height of chassis as it drives over muddy terrain.

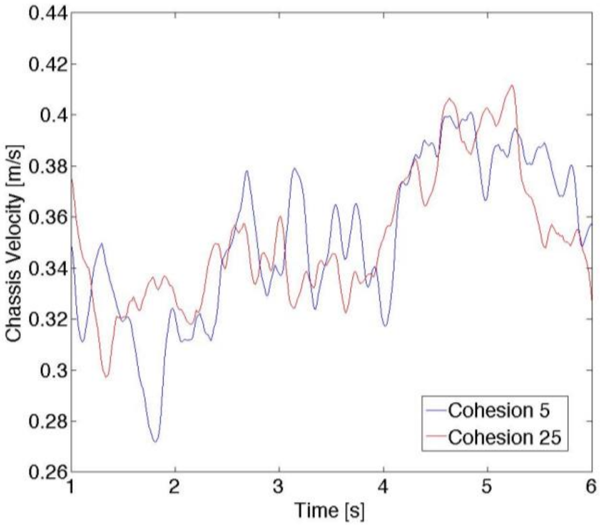

Figure 11: Chassis velocity as it drives over muddy terrain

4.3 Gravel Slope Investigation

Several simulations were performed to investigate the wheeled vehicle's ability to climb the gravel hill in Figure 7. The vehicle was aimed directly at the hill and propelled with a constant torque. The slope of the hill was varied to determine what grade the wheel vehicle could handle.

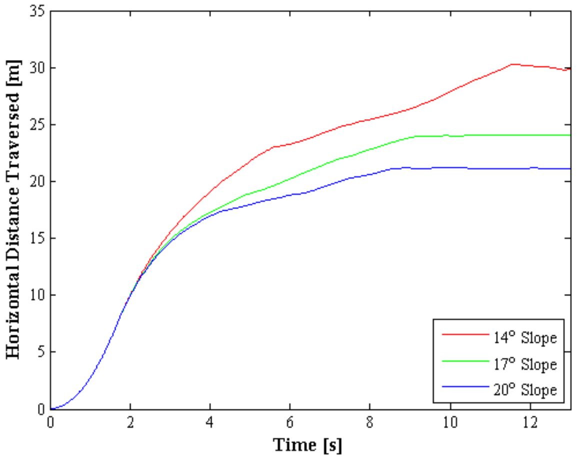

Figure 12: Horizontal distance that the Humvee has traversed over time as a function of the rocky hill slope.

The horizontal distance of the vehicle is plotted over time, shown in Figure 12. Three simulations were performed with the slope of the hill ranging from 14° to 20°. The wheeled vehicle starts at zero velocity and increases velocity on a flat rigid terrain due to a constant torque applied to the rear wheels. The wheeled vehicle hits the slope at approximately two seconds, causing the vehicle to lose velocity. For steep slopes, the wheeled vehicle cannot surmount the hill and gets stuck. As the slope decreases, the vehicle is able to make it farther and faster up the slope. The simulation was performed on a single core of an Intel Nehalem Xeon E5520 2.26 GHz processor. The simulation took approximately 45 minutes to compute 30 seconds of vehicle dynamics.

4.4 River Fording Investigation

Simulations were performed with various amounts of particles and particle sizes in order to better understand how the vehicle interacts with the fluid as it enters and exits the section of river. For results of these simulations see Figure 13. These simulations show that when the height of the water is below the chassis, the water does not resist the vehicles motion and the wheels cut through easily. As the water level increases and it comes into contact with the chassis, a large wave in front of the vehicle forms as the vehicles pushes through the water. If the level is too high the fluid would likely enter the engine and crew compartments.

5 Summary

This paper describes a modeling, simulation, and visualization framework aimed at enabling physics-based analysis of ground vehicle mobility. The framework, called Chrono, has been built to leverage parallel computing both on distributed and shared memory architectures. The code is designed to support the simulation of large systems of equations associated with the modeling of terrain via discrete bodies, where the number of interacting elements can be in the millions. While Chrono requires a small number of model parameters, allows for numerical integration at large step-sizes, and robustly handles the discontinuities in velocities, it calls for more involved mathematical instruments both in the equation formulation and equation solution stages. The increased numerical solution computational pressure is alleviated by the use of parallel hardware architectures that reduce run times for large simulation problems. Several difficult mobility situations: urban operations, muddy terrain operations, gravel slope operations, and river fording, were simulated and several sample engineering studies were demonstrated to show the types of output that can be produced by Chrono for military applications and ground mobility studies.

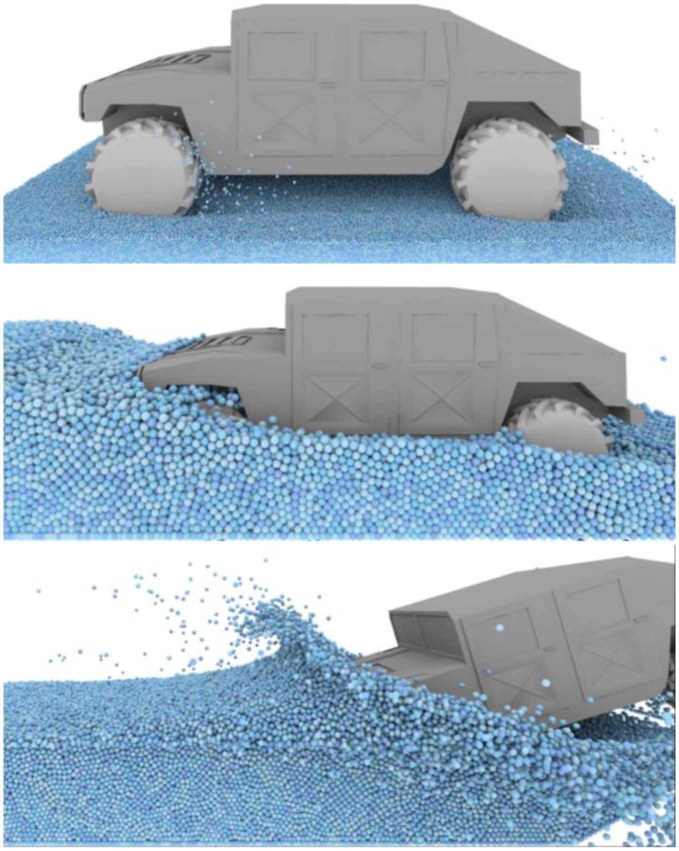

Figure 13: Vehicle traversing river section for various water heights. The first image shows a simulation with small fluid particles and a very low river depth. The second image shows a medium depth with the vehicle able to traverse the river. The last image shows a deep river and the vehicle creating as bow wave as it enters.

6 Acknowledgments

Financial support for this work was provided in part by National Science Foundation, through grant NSF CMMI-084044 and through Army Research Office grants W911NF-11-1-0327 and W911NF-12-1-0395. Nvidia is acknowledged for providing the GPU hardware used in generating the simulation results reported herein.

7 References

[1] M. Bekker, *Theory of land locomotion: the mechanics of vehicle mobility*. 1956.

[2] J. Wong and A. Reece, "Prediction of rigid wheel performance based on the analysis of soil-wheel stresses part I. Performance of driven rigid wheels," *J. Terramechanics*, vol. 4, no. 1, 1967.

[3] G. Meirion-Griffith and M. Spenko, "A modified pressure–sinkage model for small, rigid wheels on deformable terrains," *J. Terramechanics*, vol. 48, no. 2, pp. 149–155, Apr. 2011.

[4] J. Madsen, D. Negrut, A. Reid, A. Seidl, P. Ayers, G. Bozdech, J. Freeman, and J. O'Kins, "A Physics-Based Vehicle/Terrain Interaction Model for Soft Soil Off-Road Vehicle Simulations," Apr. 2012.

[5] EDEM, "Discrete Element Method Simulation Software." [Online]. Available: http://www.dem-solutions.com/software/edem-software/.

[6] ITASCA, "Discrete Element Method Simulation Software." [Online]. Available: http://www.itascacg.com/software.

[7] E. Haug, *Computer-Aided Kinematics and Dynamics of Mechanical Systems, Volume I: Basic Methods*. Boston: Allen and Bacon, 1989.

[8] E. Hairer and G. Wanner, *Solving Ordinary Differential Equations II: Stiff and Differential-Algebraic Problems*, Second Rev., vol. 14. Berlin: Springer, 1996.

[9] A. Shabana, *Dynamics of multibody systems*. Cambridge: Cambridge University Press, 2005.

[10] MSC Software, "ADAMS: The Multibody Dynamics Simulation Solution." [Online]. Available: http://www.mscsoftware.com/product/adams.

[11] INTEC GmbH, "SIMPACK MBS Software." [Online]. Available: http://www.simpack.com/.

[12] FunctionBay, "RecurDyn Multi-Body Simulation Software." [Online]. Available: http://eng.functionbay.co.kr/.

[13] J. Madsen, N. Pechdimaljian, and D. Negrut, "Penalty Versus Complementary-Based Frictional Contact of Rigid Spheres : a CPU Time Comparison," *Simulation-Based Eng. Lab.*, 2007.

[14] L. Fang and D. Negrut, "Scaling Analysis of a Penalty Approach For Multibody Dynamics with Friction and Contact," *Simulation-Based Eng. Lab.*, 2013.

[15] "Project Chrono: An Open Source Framework for the Physics-Based Simulation of Dynamic Systems," 2013. [Online]. Available: http://www.projectchrono.org/.

[16] A. Fillipov, *Differential Equations with Discontinuous Righthand Sides - Control Systems*. Norwell, MA: Kluwer Academic, 1988.

[17] D. Stewart, "Rigid-body dynamics with friction and impact," *SIAM Rev.*, vol. 42, no. 1, pp. 3–39, Jan. 2000.

[18] D. Stewart and J. C. Trinkle, "An implicit time-stepping scheme for rigid body dynamics with coulomb friction," *Robot. Autom. 2000. ...*, vol. 1, pp. 162–169, 2000.

[19] M. Anitescu and A. Tasora, "An iterative approach for cone complementarity problems for nonsmooth dynamics," *Comput. Optim. Appl.*, 2010.

[20] A. Tasora, D. Negrut, and M. Anitescu, "GPU-based parallel computing for the simulation of complex multibody systems with unilateral and bilateral constraints: an overview," *Multibody Dyn.*, 2011.

[21] D. Bertsekas, *Nonlinear Programming*. Athena Scientific, 1999.

[22] F. Pfeiffer, *Multibody Dynamics with Unilateral Contacts*. John Wiley & Sons, 1996, p. 317.

[23] J. Moreau and M. Jean, “Numerical treatment of contact and friction: the contact dynamics method,” *1996 3 rd Bienn. Jt. Conf. …*, 1996.

[24] E. Hairer, C. Lubich, and G. Wanner, *Geometric numerical integration: structure-preserving algorithms for ordinary differential equations*. 2006.

[25] J. Pang and J. Trinkle, “Complementarity formulations and existence of solutions of dynamic multi-rigid-body contact problems with Coulomb friction,” *Math. Program.*, 1996.

[26] J. Trinkle and J. Pang, “On Dynamic Multi-Rigid-Body Contact Problems with Coulomb Friction,” *Zeitschrift fur Angew. Math. und Mech.*, 1997.

[27] M. Anitescu and F. Potra, “Formulating dynamic multi-rigid-body contact problems with friction as solvable linear complementarity problems,” *Nonlinear Dyn.*, no. 93, pp. 1–21, 1997.

[28] M. Anitescu, “Optimization-based simulation of nonsmooth rigid multibody dynamics,” *Math. Program.*, 2006.

[29] D. Negrut, A. Tasora, M. Anitescu, and H. Mazhar, “Solving large multi-body dynamics problems on the GPU,” *GPU Gems*, pp. 1–33, 2011.

[30] M. Anitescu and G. Hart, “A fixed-point iteration approach for multibody dynamics with contact and small friction,” *Math. Program.*, vol. 101, no. 1, Jul. 2004.

[31] M. Anitescu and G. Hart, “A constraint-stabilized time-stepping approach for rigid multibody dynamics with joints, contact and friction,” *Int. J. Numer. …*, pp. 1–6, 2004.

[32] D. Melanz, M. Tupy, B. Smith, K. Turner, and D. Negrut, “On the Validation of a Differential Variational Inequality Approach for the Dynamics of Granular Material,” 2009.

[33] D. Melanz, M. Tupy, B. Smith, K. Turner, and D. Negrut, “On the Validation of a Differential Variational Inequality Approach for the Dynamics of Granular Material,” pp. 1–13, 2010.

[34] T. Heyn, “On the modeling, simulation, and visualization of many-body dynamics problems with friction and contact,” 2013.

[35] M. Ambroso, R. Kamien, and D. Durian, “Dynamics of shallow impact cratering,” *Phys. Rev. E*, pp. 1–4, 2005.

[36] R. Glenn, “Combat in Hell: A Consideration of Constrained Urban Warfare,” 1996.

[37] M. Babilot, “Comparison of a distributed operations force to a traditional force in urban combat,” no. September, 2005.

[38] S. Das, “Situation assessment in urban combat environments,” *2005 7th Int. Conf. Inf. Fusion*, p. 2 pp., 2005.

[39] R. Yang, M. Xu, X. Liang, S. Zhang, Y. Cheng, H. Xu, and J. Yang, “Experimental study and DEM analysis on rigid driving wheel’s performance for off-road vehicles moving on loose soil,” *2011 IEEE Int. Conf. Mechatronics Autom.*, pp. 142–147, Aug. 2011.

[40] V. Salokhe, D. Gee-Clough, and S. Manzoor, “Studies on effect of surface coating on forces produced by cage wheel lugs in wet clay soil,” *J. Terramechanics*, vol. 27, no. 2, pp. 145–157, 1990.

[41] S. Peters and K. Iagnemma, “Mobile robot path tracking of aggressive maneuvers on sloped terrain,” *Intell. Robot. Syst. 2008. …*, pp. 22–26, 2008.

[42] A. Grečenko, “Operation on steep slopes: State-of-the-art report,” *J. Terramechanics*, vol. 21, no. 2, pp. 181–194, 1984.

[43] B. Mashadi and H. Nasrolahi, “Automatic control of a modified tractor to work on steep side slopes,” *J. Terramechanics,* vol. 46, no. 6, pp. 299–311, Dec. 2009.

[44] D. Sloss and W. Baker, “The military water-crossing problem,” *J. Terramechanics,* vol. 4, no. 4, 1967.

[45] A. Bird, “The river—An unresolved obstacle,” *J. Terramechanics*, vol. 5, no. 4, pp. 51–57, 1968.

[46] A. J. Rymiszewski, “Improving the water speed of wheeled vehicles,” *J. Terramechanics*, vol. 1, no. 1, pp. 75–90, Jan. 1964.